Journal of ELECTRONIC MATERIALS, Vol. 49, No. 10, 2020
https://doi.org/10.1007/s11664-020-08337-x

Triple-Band Terahertz Perfect Light Absorber Using the Strong Interaction of Two Metallic Resonators

BEN-XIN WANG,[1,4] CHAO TANG,[1] QINGSHAN NIU,[1] YUANHAO HE,[1] FUWEI PI,[2] and XIAOYI WANG[3,5]

1.—School of Science, Jiangnan University, Wuxi 214122, China. 2.—State Key Laboratory of Food Science and Technology, School of Food Science and Technology, Jiangnan University, Wuxi 214122, China. 3.—Key Laboratory of Optical System Advanced Manufacturing Technology, Changchun Institute of Optics, Fine Mechanics and Physics, Chinese Academy of Sciences, Changchun 130033, China. 4.—e-mail: wangbenxin@jiangnan.edu.cn. 5.—e-mail: wangxiaoyi@ciomp.ac.cn

An approach to realize a multiple-band perfect light absorber is demonstrated using a simple metamaterial design featuring a composite metallic structure consisting of a closed ring and a rectangular patch atop a metallic substrate separated by an insulator. Three narrow-band and discrete resonance peaks with nearly 100% absorption rates are obtained. The first absorption peak is due to the dipole resonance of the closed ring, while the last two absorption peaks are caused by the coupling effect of the closed ring and rectangular patch. The field distribution of the three absorption peaks is given to provide additional evidence. Unlike traditional multiple-band light absorbers that eliminate (or avoid) the interaction between the metallic array structures, our design is based on the mode coupling of the composite structure. This method can obviously reduce the number of metallic resonators, simplify the structure design and reduce fabrication costs.

Key words: Terahertz metamaterial, perfect absorber, triple-band absorption, strong coupling

INTRODUCTION

Over the past few years, studies on metamaterials have attracted wide interest from a vast number of researchers owing to their remarkable and exotic properties that cannot be directly obtained in natural materials. These properties include a negative refractive index,[1] electromagnetic stealth and cloaking,[2] and a perfect lens.[3] However, these demonstrations on metamaterials are mainly focused on the acquisition of novel and exotic physical properties, and are not linked to the functional device designs. It has been reported that metamaterials have enormous potential applications and business opportunities in functional devices. This is why we have witnessed the explosive development of functional devices based on metamaterials in recent years.[4–9] Metamaterial perfect light absorbers,[9] as a typical representative of functional devices, have become the latest research hotspot because of their strong absorption capacity and ultra-thin insulator thickness.

The design scheme of the perfect light absorber consisting of two metallic pattern structures separated by an insulator was firstly demonstrated by researchers from Boston College in 2008.[9] A single resonance absorption peak with the absorbance of 96% at a frequency of 11.5 GHz can be obtained in this sandwich structure. More importantly, the thickness of the insulator used in this microwave absorber is only 1/35 of the given resonance wavelength,[9] which is far less than that of the electromagnetic devices of a Salisbury screen[10] and Jaumann absorber[11] with the 1/4 resonance wavelength. As a result, the suggested metamaterial absorber can significantly reduce the thickness of the

(Received October 22, 2019; accepted July 16, 2020; published online July 28, 2020)

resonance device, thereby reducing the costs of fabrication and processing, as well as the merit of being lightweight. Due to these remarkable advantages, metamaterial absorbers have been extensively studied in recent years, and their working frequencies are no longer limited to the microwave bands and have been gradually extended to every technology-related frequency domain.[12–20] Unfortunately, these reported metamaterial absorbers have only one resonance absorption peak (or single-band absorption). This is highly disadvantageous in many practical applications.

To overcome the shortcomings of single-band absorption, it is necessary to increase the number of absorption peaks. To this end, many researchers have made significant efforts to design multiple-band metamaterial absorbers.[21–54] From the perspective of the number of resonance peaks, these multiple-band metamaterial absorbers can be divided into dual-band absorption, triple-band absorption, and even quad-band absorption. Two different-sized metallic resonators[21–24] and four metallic resonators with two sets of different sizes[25–29] were suggested to realize dual-band absorption. In these structures, each resonator has only one resonance absorption peak, and thus the superposition effect of two absorption peaks with discrete resonance frequencies gives rise to dual-band absorption. Taking into account this design idea, triple-band absorption and even quad-band absorption can be easily obtained by employing a greater number of metallic elements having different dimensions.[30–45] For example, the use of three concentric closed-ring resonators,[30,31] four or five metallic elements,[32–34] eight closed-ring resonators with four sets of concentric structures,[35] and even nine elements with three sets of different sizes[36–40] has been able to achieve triple-band absorption.

In this paper, we employ the coupling and interaction of two differently shaped resonators to achieve the triple-band light absorber. The two resonators are the closed-ring resonator and rectangular patch, which are connected to form the metallic composite structure. Three narrow-band and discrete resonance modes with nearly 100% absorbance at terahertz frequency are realized. The near-field distribution of the three absorption bands provides insight into the physical origin of the triple-band absorption. It is revealed that the first absorption peak is derived from the dipole resonance of the closed ring, while the last two absorption modes come from the strong interaction between the two resonators. The influence of structure parameters on its absorption performance can provide additional explanation for the resonance mechanism.

STRUCTURE DESIGN AND MODEL

The triple-band terahertz absorber consisting of three functional layers is illustrated in Fig. 1a. The first and third functional layers are both made of Au, whose conductivity is $\sigma = 4.09 \times 10^7$ S/m, and are separated by an insulator with thickness of $t = 12$ μm and dielectric constant of $3(1 + i0.05)$. The roles of the two Au layers are different. The first one provides the strong interaction with the incident waves, while the second serves as the substrate, which can completely block the light. The first Au layer is actually a composite structure consisting of a closed ring and rectangular patch (see Fig. 1b). The closed ring has the same size of $a = 80$ μm in length and width, and its line width is $w = 5$ μm. The rectangular patch has a length of $l = 30$ μm and width of $d = 60$ μm. The metallic composite structure is placed on the unit cell with the period of $P = 100$ μm. The finite difference time domain method with the appropriate boundary conditions is used to simulate its absorption performance. The incident light source is a plane-wave beam with the direction of x-axis polarization, which is perpendicular to the array along the + z direction.

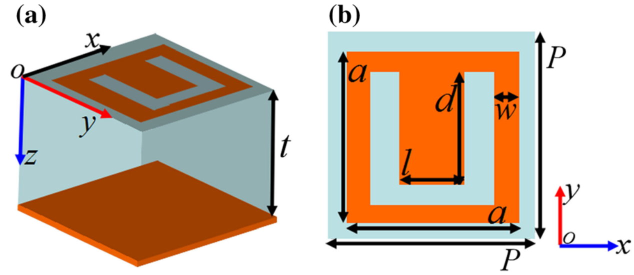

Fig. 1. (a) Three-dimensional schematic diagram of triple-band metamaterial absorber. (b) Two-dimensional schematic diagram of triple-band metamaterial absorber.

RESULTS AND DISCUSSION

Figure 2a exhibits the absorption curve of the designed absorber under the vertical radiation of the light beam. It is observed that three sharp resonance peaks with nearly 100% absorbance are obtained. The first absorption peak is localized at R1 = 0.67 THz, while the frequencies of the last two bands are localized at R2 = 2.00 THz and R3 = 2.29 THz. Compared to previous triple-band metamaterial absorbers with many different sizes of resonators (see Table I), the structure designed here requires only two connected resonators to achieve triple-band absorption performance, which could provide for better structure optimization and design. Results further demonstrate that the absorption bandwidths of the three modes are all smaller than 0.10 THz. These properties, including multiple absorption bands, large absorbance, narrow bandwidth, and simple structural design, are quite important in practical applications.

In previous designs, it has generally been impossible to achieve triple-band absorption using two metallic resonators. Therefore, we predict that a coupling effect between the two resonators should exist, and only the existence of coupling can realize this kind of abnormal resonance performance. To

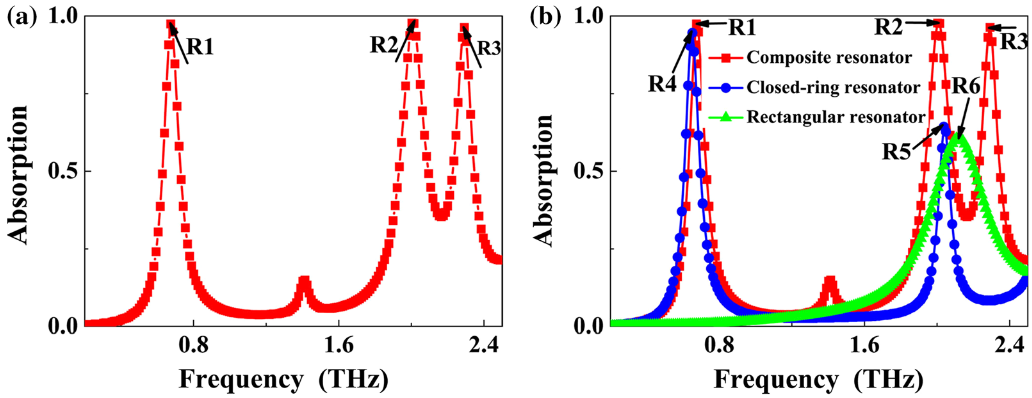

Fig. 2. (a) Resonance absorption curve of triple-band metamaterial absorber; (b) curves of red, blue, and green are respectively the absorption response of the metamaterial absorber with a metallic composite structure, a closed ring, and a rectangular patch (Color figure online).

Table I. Comparison between the designed triple-band metamaterial absorber and previous ones

References	Number of sub-resonators	Coupling considered?	Physical mechanism	Absorption peaks	Construction steps
30	3	No	Mode superposition	Independently adjustable	Complex
31	3	No	Mode superposition	Independently adjustable	Complex
32	4	No	Mode superposition	Independently adjustable	Complex
33	4	No	Mode superposition	Independently adjustable	Complex
34	5	No	Mode superposition	Independently adjustable	Complex
35	8	No	Mode superposition	Independently adjustable	Complex
36	9	No	Mode superposition	Independently adjustable	Complex
37	9	No	Mode superposition	Independently adjustable	Complex
38	9	No	Mode superposition	Independently adjustable	Complex
39	9	No	Mode superposition	Independently adjustable	Complex
40	9	No	Mode superposition	Independently adjustable	Complex
This work	2	Yes	Mode coupling	Mutual restriction	Simple

determine the existence of the coupling and the specific circumstances of coupling, we present the absorption curves of the absorbers with a closed ring and a rectangular patch. Note that the parameters of the absorber with a closed ring (or rectangular patch) are the same as those of the absorber with the composite structure in Fig. 1, except that there is no rectangular patch (or no closed ring).

It can be seen from the blue curve in Fig. 2b that there are two absorption bands (marked as R4 and R5) for the absorber with the closed ring, while only one resonance mode (marked as R6) is found for the absorber having the rectangular patch (see the green curve of Fig. 2b). Compared with three absorption modes (R1, R2, and R3) in the red curve of Fig. 2b, two points can be observed clearly. Firstly, the mode R4 is very close to the absorption band R1, which means that the mechanism of mode R1 should be the same as that of mode R4. Secondly, the resonance frequency of mode R6 is close to that of mode R5. However, the properties (including the resonance frequency and the absorbance) of modes R5 and R6 are both different from the last two absorption modes R2 and R3, indicating that the mechanism of modes R2 and R3 is caused by the coupling of the closed ring and rectangular patch. On the basis of the above analysis, we know that the operating mechanism of mode R1 should result from the first mode (R4) of the closed ring, while the formation of modes R2 and R3 should be attributed to the coupling between the closed ring and rectangular patch.

To analyze the physical mechanisms of modes R1, R2, and R3, it is necessary to investigate the origins of modes R4 and R5 of the closed ring and R6 of the rectangular patch. It can be seen from Fig. 3a that the $|E|$ field of mode R4 is mostly concentrated on the edges of the closed ring; its Ez field in Fig. 3b exhibits the similar distribution characteristic that is gathered in both sides of the closed ring. These field patterns prove that mode R4 is due to the dipole resonance of the closed ring. Correspondingly, the mechanism of mode R6 should be the dipole resonance of the rectangular patch, because its $|E|$ and Ez fields are both distributed at both sides of the rectangular patch (see Fig. 3e and f). Because the length of the closed ring differs from that of the rectangular patch, their frequencies are

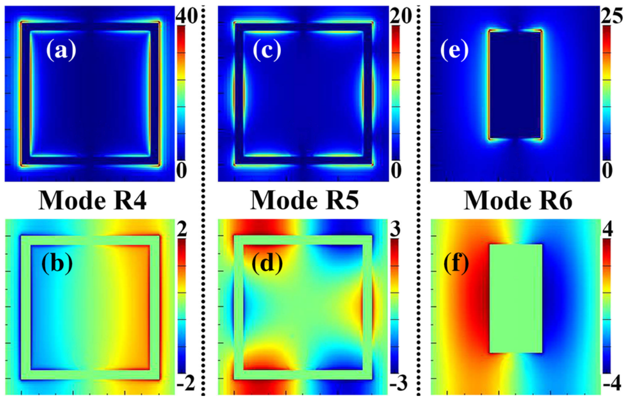

Fig. 3. (a) and (b) are respectively the |*E*| and *Ez* field profiles of mode R4; (c) and (d) are respectively the |*E*| and *Ez* field profiles of mode R5; (e) and (f) are respectively the |*E*| and *Ez* field profiles of mode R6.

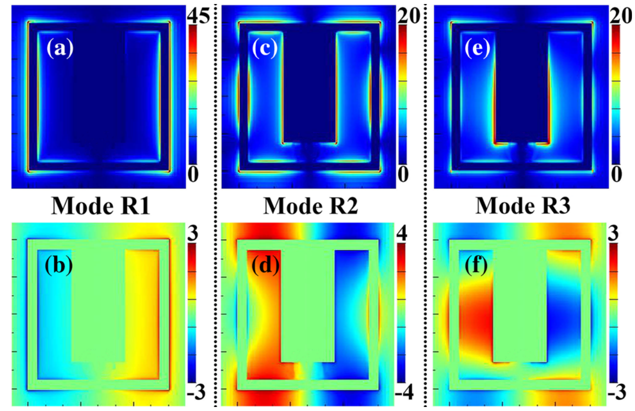

Fig. 4. (a) and (b) are respectively the |*E*| and *Ez* field profiles of mode R1 of the triple-band metamaterial absorber; (c) and (d) are respectively the |*E*| and *Ez* field profiles of mode R2 of the triple-band metamaterial absorber; (e) and (f) are respectively the |*E*| and *Ez* field profiles of mode R3 of the triple-band metamaterial absorber.

different. Furthermore, the field distribution of the second mode (i.e., mode R5) of the closed ring in Fig. 3c and d is mainly clustered in both middle sides along the electric field direction and the corners of the closed ring, which indicate that mode R5 is caused by the quadrupole resonance in the closed ring.

We next give the field distribution of the three resonance modes R1, R2, and R3 to investigate their formation mechanisms. As revealed in Fig. 4a and b, the |*E*| and *E*z fields of mode R1 are primarily concentrated on both edges of the closed ring, while the fields in the rectangular patch are neglected. The fields of mode R1 are very similar to those of mode R4 of the closed ring in Fig. 3a and b, indicating that mode R1 is the dipole resonance of the closed ring. For modes R2 and R3 (see Fig. 4c–f), their fields are both focused not only on the edges of the closed ring but also on the edges of the rectangular patch, showing that the coupling between the two resonators gives rise to the two resonance modes. Furthermore, the fields of mode R2 in Fig. 4c and d (or mode R3 in Fig. 4e and f) are accumulated at the four corners and both middle sides of the closed ring, which show the quadrupole resonance performance. For the rectangular patch, it is observed that the fields of modes R2 and R3 are both focused on both sides of its own structure, and this clearly exhibits the characteristic of dipole resonance. Therefore, the mechanisms of modes R2 and R3 in the metallic composite structure mainly result from the coupling of the quadrupole resonance in the closed ring and the dipole resonance in the rectangular patch. However, the gather intensity of the fields of these two modes in specific positions is different. As observed in Fig. 4c–f, the field distribution intensity of mode R2 in the edges of the closed ring is larger than that of mode R3 in the same positions of the closed ring, while the field gather intensity of mode R2 in both sides of rectangular patch is smaller than that of mode R3 in the same positions. As a result, modes R2 and R3 should be attributed to the different coupling intensity of quadrupole resonance of the closed ring and dipole resonance of the rectangular patch.

Table I shows the comparison between the designed absorber and previous ones. Previously reported absorbers usually have a large number of sub-resonators. So many sub-resonators gathering in the unit cell will inevitably lead to some issues, such as time-consuming structure optimization, cumbersome construction steps, and high cost. More importantly, these absorbers try to avoid the coupling between the sub-resonators and use the superposition effect of the localized resonance mode of sub-resonators themselves to achieve the triple-band absorption. It would be quite interesting to introduce some coupled (or interacted) resonators in the design of triple-band absorbers. The introduction of coupling between the sub-resonators can generally reduce the number of sub-resonators, thereby solving the issues encountered in previous absorbers. In other words, the absorber designed here using only two coupled sub-resonators is totally different from previous ones; therefore, many potential applications could be found for the suggested absorber. Although previously reported absorbers have some disadvantages, they share common features that their absorption peaks could be independently adjusted, which is not possible in this manuscript. The main reason is that the physical mechanism of the designed absorber is mainly attributed to the strong interaction between the sub-resonators, and therefore slight changes in the structure should significantly affect all absorption peaks.

The changes of structure parameters can provide additional evidence to analyze the physical origin of the three absorption peaks. As revealed in Fig. 5a, the length change of the rectangular patch shows the obvious ability to control modes R2 and R3,

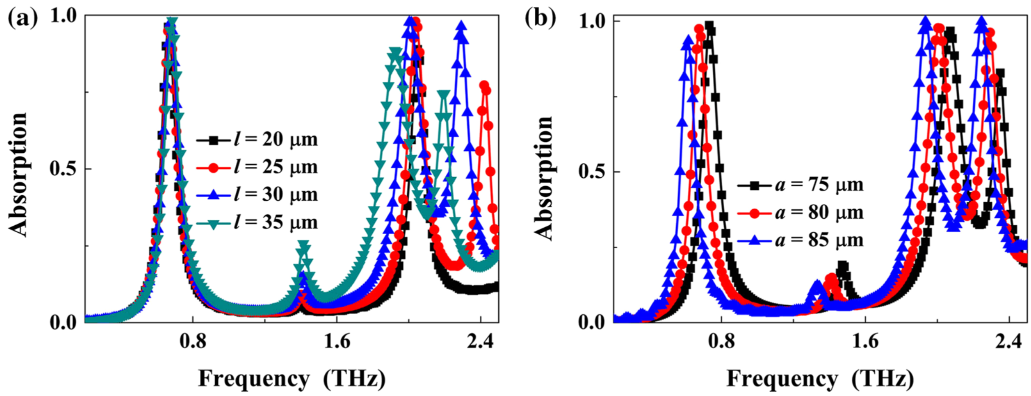

Fig. 5. (a) Absorption curves of triple-band metamaterial absorber with length (l) changes of rectangular patch; (b) absorption curves of triple-band metamaterial absorber with the length (a) changes of closed ring.

while mode R1 is nearly unchanged because its field distribution in the rectangular patch is very weak and can be negligible. Furthermore, there may be some absorption peaks which are not part of the frequency range of interest because the frequencies of modes R2 and R3 are intensely influenced by the length (l). For l = 20 μm, there are only two absorption peaks, which means that the designed structure has the ability to tune the number of absorption peaks when the length l is varied. Additionally, according to the field profiles of modes R1, R2, and R3, it is predicted that the length change of the closed ring should affect the performance of all absorption peaks. As shown in Fig. 5b, the properties of the three absorbers are indeed strongly controlled by the length of the closed ring.

CONCLUSION

In conclusion, we present a scheme to achieve the simple design of a multiple-band metamaterial absorber at terahertz frequency using a metallic composite structure consisting of a closed ring and rectangular patch atop a metallic substrate separated by an insulator. Three nearly 100% absorption peaks with narrow bandwidths are realized. The first absorption peak with lower frequency results from the dipole resonance of the closed ring, while the last two absorption bands are caused by different coupling of quadrupole resonance in the closed ring and dipole resonance in the rectangular patch. The influence of dimension changes in the composite structure on the resonance performance of the metamaterial absorber is discussed. Compared with prior multiple-band absorbers using many sub-resonators, the suggested device has the obvious merits of simple structural design, a small number of sub-resonators, and novel physical mechanism. These factors are quite important in designing multiple-band absorbers, and thus the given absorption device could have considerable potential for application in terahertz technology.

ACKNOWLEDGMENTS

This research was funded by the National Natural Science Foundation of China (21603087, 11647143), Natural Science Foundation of Jiangsu Province (BK20160178, BK20160189), China Postdoctoral Science Foundation (2019M651692), Jiangsu Postdoctoral Science Foundation (2018K113C), Fundamental Research Funds for Central Universities (JUSRP51721B), Open Fund of Key Laboratory of Optical System Advanced Manufacturing Technology, and Chinese Academy of Sciences (KLOMT190103).

CONFLICT OF INTEREST

The authors declare that they have no conflict of interest.

REFERENCES

1. D.R. Smith, J.B. Pendry, and M.C.K. Wiltshire, *Science* 305, 788 (2004).
2. D. Schurig, J.J. Mock, B.J. Justice, S.A. Cummer, J.B. Pendry, A.F. Starr, and D.R. Smith, *Science* 314, 977 (2006).
3. J.B. Pendry, *Phys. Rev. Lett.* 85, 3966 (2000).
4. M. Lu, W. Li, and E.R. Brown, *Opt. Lett.* 36, 1071 (2011).
5. S. Zhang, D.A. Genov, Y. Wang, M. Liu, and X. Zhang, *Phys. Rev. Lett.* 101, 047401 (2008).
6. P. Jung, S. Butz, M. Marthaler, M.V. Fistul, K. Leppakangas, V.P. Koshelets, and A.V. Ustinov, *Nat. Commun.* 5, 3730 (2014).
7. N.I. Zheludev and Y.S. Kivshar, *Nat. Mater.* 11, 917 (2012).
8. H.T. Chen, W.J. Padilla, M.J. Cich, A.K. Azad, R.D. Averitt, and A.J. Taylor, *Nat. Photon.* 3, 148 (2009).
9. N.I. Landy, S. Sajuyigbe, J.J. Mock, D.R. Smith, and W.J. Padilla, *Phys. Rev. Lett.* 100, 207402 (2008).
10. B.A. Munk, *Frequency Selective Surfaces: Theory and Design* (New York: Wiley, 2000), pp. 315–319.
11. W.W. Salisbury, US Patent, 2599944 (1952).
12. H.T. Chen, *Opt. Express* 20, 7165 (2012).
13. X. Liu, K. Bi, B. Li, Q. Zhao, and J. Zhou, *Opt. Express* 24, 20454 (2016).
14. I. Faniayeu and V. Mizeikis, *Appl. Phys. Express* 10, 062001 (2017).
15. B.X. Khuyen, B.S. Tung, Y.J. Yoo, Y.J. Kim, K.W. Kim, L.Y. Chen, V.D. Lam, and Y.P. Lee, *Sci. Rep.* 7, 45151 (2017).
16. M. Wu, X. Zhao, J. Zhang, J. Schalch, G. Duan, K. Cremin, R.D. Averitt, and X. Zhang, *Appl. Phys. Lett.* 111, 051101 (2017).

17. X. Zhao, J. Zhang, K. Fan, G. Duan, G.D. Metcalfe, M. Wraback, X. Zhang, and R.D. Averitt, *Photonics Res.* 4, A16 (2016).
18. S. Tan, F. Yan, W. Wang, H. Zhou, and Y. Hou, *J. Opt.* 20, 055101 (2018).
19. K. Bhattarai, Z. Ku, S. Silva, J. Jeon, J.O. Kim, S.J. Lee, A. Urbas, and J. Zhou, *Adv. Opt. Mater.* 3, 1779 (2015).
20. C.Y. Yang, J.H. Yang, Z.Y. Yang, Z.X. Zhou, M.G. Sun, V.E. Babicheva, and K.P. Chen, *ACS Photonics* 5, 2596 (2018).
21. W. Zhang, F. Lan, J. Xuan, P. Mazumder, M. Aghadjani, Z. Yang, and L. Meng, *IEEE MTT-S International Microwave Workshop Series on Advanced Materials and Processes*, 20–22 September 2017, Pavia, Italy.
22. Y. Ma, Q. Chen, J. Grant, S.C. Saha, A. Khalid, and D.R.S. Cumming, *Opt. Lett.* 36, 945 (2011).
23. J. Kim, K. Han, and J.W. Hahn, *Sci. Rep.* 7, 6740 (2017).
24. M. Zhang, G.M. Han, S.J. Liu, B.L. Xu, J. Wang, and H.Q. Huang, *Physica E* 86, 158 (2017).
25. X. Liu, C. Lan, K. Bi, B. Li, Q. Zhao, and J. Zhou, *Appl. Phys. Lett.* 109, 062902 (2016).
26. Y. Zhang, T. Li, Q. Chen, H. Zhang, J.F. Ohara, E. Abele, A.J. Taylor, H.T. Chen, and A.K. Azad, *Sci. Rep.* 5, 18463 (2015).
27. G. Yao, F. Ling, J. Yue, C. Luo, J. Ji, and J. Yao, *Opt. Express* 24, 1518 (2016).
28. X. Liu, C. Lan, B. Li, Q. Zhao, and J. Zhou, *Sci. Rep.* 6, 28906 (2016).
29. B. Zhang, Y. Zhao, Q. Hao, B. Kiraly, I.C. Khoo, S. Chen, and T.H. Huang, *Opt. Express* 19, 15221 (2011).
30. X. Shen, T.J. Cui, J. Zhao, H.F. Ma, W.X. Jiang, and H. Li, *Opt. Express* 19, 9401 (2011).
31. X. Shen, Y. Yang, Y. Zang, J. Gu, J. Han, W. Zhang, and T.J. Cui, *Appl. Phys. Lett.* 101, 154102 (2012).
32. S. Bhattacharyya and K.V. Srivastava, *J. Appl. Phys.* 115, 064508 (2014).
33. F.S. Jafari, M. Naderi, A. Hatami, and F.B. Zarrabi, *Int. J. Electron. Commun. (AEU)* 101, 138 (2019).
34. X. Huang, H. Yang, S. Yu, J. Wang, M. Li, and Q. Ye, *J. Appl. Phys.* 113, 213516 (2013).
35. S. Bhattacharyya, S. Ghosh, and K.V. Srivastava, *J. Appl. Phys.* 114, 094514 (2013).
36. H. Li, L.H. Yuan, B. Zhou, X.P. Shen, Q. Cheng, and T.J. Cui, *J. Appl. Phys.* 110, 014909 (2011).
37. H. Zhai, C. Zhan, Z. Li, and C. Liang, *IEEE Antennas Wirel. Propag. Lett.* 14, 241 (2015).
38. T.M. Kollatou, A.I. Dimitriadis, S.D. Assimonis, N.V. Kantartzis, and C.S. Antonpoulos, *Appl. Phys. A* 115, 555 (2014).
39. J. Chen, Z. Hu, S. Wang, X. Huang, and M. Liu, *Eur. Phys. J. B* 89, 14 (2016).
40. B. Zhang, J. Hendrickson, and J. Guo, *J. Opt. Soc. Am. B* 30, 656 (2013).
41. M. Agarwal, A.K. Behera, and M.K. Meshram, *Electron. Lett.* 52, 340 (2016).
42. S. Liu, J. Zhuge, S. Ma, H. Chen, D. Bao, Q. He, L. Zhou, and T.J. Cui, *J. Appl. Phys.* 118, 245304 (2016).
43. B.X. Wang, X. Zhai, G.Z. Wang, W.Q. Huang, and L.L. Wang, *IEEE Photonics J.* 7, 4600108 (2015).
44. L. Wang, C. Hu, X. Wu, Z. Xia, and W. Wen, *Appl. Phys. A* 123, 651 (2017).
45. Y.H. Ren, J. Ding, C.J. Guo, Y. Qu, and Y.C. Song, *J. Electron. Mater.* 46, 370 (2016).
46. B.X. Wang, *IEEE J. Select. Top. Quantum Electron.* 23, 4700107 (2017).
47. B.X. Wang, G.Z. Wang, and T. Sang, *J. Phys. D Appl. Phys.* 49, 165307 (2016).
48. B.X. Wang, G.Z. Wang, and L.L. Wang, *Plasmonics* 11, 523 (2016).
49. B.X. Wang, Y. He, P. Lou, W.Q. Huang, and F. Pi, *Results Phys.* 16, 102930 (2020).
50. B.X. Wang, Y. He, P. Lou, and W. Xing, *Nanoscale Adv.* 2, 763 (2020).
51. B.X. Wang and G.Z. Wang, *Plasmonics* 13, 123 (2018).
52. B.X. Wang, G.Z. Wang, L.L. Wang, and X. Zhai, *IEEE Photonics Technol. Lett.* 28, 307 (2016).
53. B.X. Wang, G.Z. Wang, T. Sang, and L.L. Wang, *Sci. Rep.* 7, 41373 (2017).
54. B.X. Wang, C. Tang, Q. Niu, Y. He, and T. Chen, *Nanoscale Res. Lett.* 14, 64 (2019).